Asymmetric coupling induces two-directional reentrance transition in three-lane exclusion process

Priyanka N. C and Atul Kumar Verma*

Department of Mathematics, National Institute of Technology, Tiruchirappalli 620015, Tamil Nadu, India

(Received 4 October 2022; revised 31 January 2023; accepted 5 March 2023; published 11 April 2023)

Inspired by vehicular traffic phenomena, we study a three-lane open totally asymmetric simple exclusion process with both-sided lane switching in the companionship of Langmuir kinetics. We calculate the phase diagrams, density profiles, and phase transitions through mean-field theory and successfully validate these findings with Monte Carlo simulation results. It has been found that both the qualitative and quantitative topology of phase diagrams crucially rely on the ratio of lane-switching rates called coupling strength. The proposed model has various unique mixed phases, including a double shock resulting in bulk-induced phase transitions. The interplay between both-sided coupling, third lane, and Langmuir kinetics produces unusual features, including a back-and-forth phase transition, also called a reentrance transition, in two directions for relatively nominal values of coupling strength. The presence of reentrance transition and peculiar phase boundaries leads to a rare type of phase division in which one phase lies entirely within another region. Moreover, we scrutinize the shock dynamics by analyzing four different types of shock and finite-size effects.

DOI: 10.1103/PhysRevE.107.044104

I. INTRODUCTION

Many natural and man-made systems evolve into nonequilibrium stationary states with steady currents under the influence of internal or external energy. Ranging from physical to biological transport, most transportation systems belong to such a category. To explain the behavior of such out-of-equilibrium processes, various kinds of lattice gas models have been proposed and examined extensively [1]. Here we concentrate on models where particles prefer to hop along a lattice only in one direction. In this direction, the totally asymmetric simple exclusion process (TASEP) has proved itself a paradigm in the area of the nonequilibrium transport system. TASEP is a stochastic model introduced by MacDonald and Gibbs in 1968 to study the kinetics of biopolymerization on nucleic acid templates [2]. In this model, a particle can enter and exit from two different ends and move in bulk with predefined rates and rules. In past decades, TASEP has been used to model and analyze numerous processes, including traffic flow, pedestrian dynamics, chains of quantum dots, movement of ants along a trail, information flow, and molecular motor traffic [3–7]. Despite being a simple model, TASEP is capable of explaining varieties of complex phenomena such as nonequilibrium phase transitions, spontaneous symmetry breaking, boundary and bulk induced transitions, shock formation, and phase separation [8–15].

Furthermore, particles can attach to or detach from the path in many systems. For instance, automobiles in a traffic system can enter (exit from) the traffic lane from (to) the side way. Similarly, in biological transport, the motor proteins' attachment and detachment occur between microtubule and cytoplasm [16]. Motivated by these examples, researchers proposed the concept of Langmuir kinetics (LK), in which a particle can join or leave the lattice bulk sites with some predefined rates. In this direction, Parmeggiani *et al.* proposed a detailed analysis of the interplay between conserving (TASEP) and nonconserving (LK) dynamics in a single-lane TASEP with LK [17,18]. It was noticed that LK produces many novel features, including phase coexistence and localization of the shock phase [13,17]. Motivated by the nontrivial impact of LK on the system dynamics, recently various studies have been conducted on single-lane TASEP-LK model [18,19].

In our daily life, we observe many systems where particles move in more than one lane. For example, vehicles travel along multiple roads forming a multilane system. Similarly, motor proteins perform the directed motion in intracellular transport along multiple protofilaments. In both instances, particles move along the numerous lanes and switch their path depending upon various situations, producing coupled multilane transport systems. Looking at the extensive appearance of coupling between paths, multiple studies have been proposed for a two-lane TASEP system with coupling between the lanes [20–22]. To analyze the traffic situations more realistically, few researchers have proposed coupled two-lane TASEP models with attachment-detachment process [23,24]. With the increase in lanes, the system becomes very complicated, leading to various challenges in extending a two-lane system to a three-lane one. Since a three-lane system is more realistic for understanding various transport systems, very few researchers have studied a complex three-lane system [11,25–29]. Wang *et al.* [11] reported a bulk-induced phase transition from the study of a three-lane TASEP with weak and asymmetric coupling. Cai *et al.* [25] studied fully asymmetric coupling in multichannel TASEP and observed that the topology of the phase diagram varies as the number of lanes increases. Jiang *et al.* [26] scrutinized the steady-state phase diagrams from

*atulv085@gmail.com

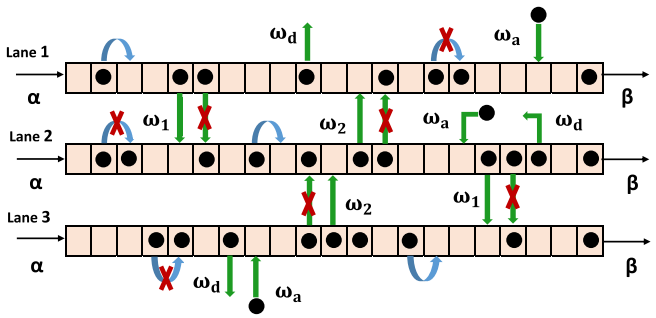

FIG. 1. Sketch of the three-lane TASEP with Langmuir kinetics. The arrows (crosses) denote permitted (prohibited) transitions. The α, β, ω_a, and ω_d correspond to entry, exit, attachment, and detachment rates. ω_1 (ω_2) denotes the coupling rate from lane 1 to lane 2, lane 2 to lane 3 (from lane 3 to lane 2, lane 2 to lane 1).

the study of multilane partially asymmetric simple exclusion process (PASEP) under a strong asymmetrically coupled environment. A few other researchers explored phase diagrams of three-lane systems under the influence of fully asymmetric coupling with Langmuir kinetics [28,29].

From the above studies of three-lane systems, it is clear that some of the studies are based on TASEP without LK [11,25–27], while studies that incorporated LK have studied only the impact of fully asymmetric coupling [28,29]. Therefore, to our knowledge, no study has explored the implications of asymmetric coupling on a three-lane TASEP system in the presence of LK. This study investigates a three-lane TASEP model coupled with LK in the presence of asymmetric coupling conditions. We wish to explore the novel phase transitions and nontrivial impact of asymmetric coupling on steady-state system dynamics of the considered model. Further, we aim to scrutinize the overall system dynamics by analyzing phase diagrams for different coupling rates.

II. MODEL DESCRIPTION AND MEAN-FIELD EQUATIONS

We consider three parallel one-dimensional open lattices denoted by lane 1, lane 2, and lane 3, as shown in Fig. 1. Each lane has exactly an N number of sites labeled as $i = 1, 2, \ldots, N$. Particles are distributed in the system under the hardcore exclusion principle, such as a site that cannot occupy more than one particle. The occupancy state of a site i is represented by a binary variable n_j^i where $j = 1, 2, 3$. The value of n_j^i is one (zero) depending on if the site is occupied (vacant) by a particle. We choose a lattice site at random at each time step and update it as per random sequential update rules. The subprocesses which govern the system dynamics are as follows:

(1) If $i = 1$, a particle can enter into the system with rate α in case n_j^1=0. If the first site is occupied, a particle can move from $i = 1$ to $i = 2$ with the unit rate provided $n_j^2 = 0$.

(2) At $i = N$, particles leave from the site with rate β provided $n_j^N = 1$.

(3) For $1 < i < N$ (bulk sites), if $n_j^i = 1$, a particle first tries to detach with rate w_d. If detachment is not possible and $n_j^{i+1} = 0$, then the particle moves to the $(i + 1)$th site. If the $(i + 1)$th site is occupied, then the particle hops to site i on lane $j + 1$ ($j - 1$) with rate ω_1 (ω_2), provided the target site is unoccupied. Clearly, ω_2 (ω_1) is 0 for lane 1 (lane 3). Besides, if the ith site is not occupied, a particle can attach to it with rate w_a.

It is to be noted that LK and lane changing do not take place at boundary sites.

We calculate the mean site occupation density for the bulk site in each lane using the following master equations:

$$\begin{aligned}\frac{d\langle n_1^i\rangle}{dt} &= \langle n_1^{i-1}(1-n_1^i)\rangle - \langle n_1^i(1-n_1^{i+1})\rangle \\ &+ \omega_a\langle 1-n_1^i\rangle - \omega_d\langle n_1^i\rangle \\ &- \omega_1\langle n_1^i n_1^{i+1}(1-n_2^i)\rangle \\ &+ \omega_2\langle n_2^i n_2^{i+1}(1-n_1^i)\rangle, \end{aligned} \tag{1}$$

$$\begin{aligned}\frac{d\langle n_2^i\rangle}{dt} &= \langle n_2^{i-1}(1-n_2^i)\rangle - \langle n_2^i(1-n_2^{i+1})\rangle \\ &+ \omega_a\langle 1-n_2^i\rangle - \omega_d\langle n_2^i\rangle \\ &- \omega_1\langle n_2^i n_2^{i+1}(1-n_3^i)\rangle - \omega_2\langle n_2^i n_2^{i+1} \\ &\times (1-n_1^i)\rangle + \omega_1\langle n_1^i n_1^{i+1}(1-n_2^i)\rangle \\ &+ \omega_2\langle n_3^i n_3^{i+1}(1-n_2^i)\rangle, \end{aligned} \tag{2}$$

$$\begin{aligned}\frac{d\langle n_3^i\rangle}{dt} &= \langle n_3^{i-1}(1-n_3^i)\rangle - \langle n_3^i(1-n_3^{i+1})\rangle \\ &+ \omega_a\langle 1-n_3^i\rangle - \omega_d\langle n_3^i\rangle \\ &+ \omega_1\langle n_2^i n_2^{i+1}(1-n_3^i)\rangle \\ &- \omega_2\langle n_3^i n_3^{i+1}(1-n_2^i)\rangle. \end{aligned} \tag{3}$$

The densities at boundaries can be calculated as follows:

$$\frac{d\langle n_j^1\rangle}{dt} = \alpha\langle(1-n_j^1)\rangle - \langle n_j^1(1-n_j^2)\rangle, \tag{4}$$

$$\frac{d\langle n_j^N\rangle}{dt} = \langle n_j^{N-1}(1-n_j^N)\rangle - \beta\langle n_j^N\rangle, \tag{5}$$

with $\langle\cdots\rangle$ as the statistical average.

To obtain the continuum limit of the model, we coarse grain the discrete lattice with lattice constant $\epsilon = \frac{1}{N}$ and rescaled time as $t' = \frac{t}{N}$. In order to explore the competition between boundary and bulk dynamics, involved bulk rates are rescaled as $\omega_a N = \Omega_a$, $\omega_d N = \Omega_d$, $\omega_1 N = \Omega_1$, $\omega_2 N = \Omega_2$.

After replacing the discrete variable $< n_j^i >$, with ρ_j^i continuous variables, in Taylor series expansion of $\rho_j^{i\pm1}$, we keep the terms up to second order resulting in

$$\rho_j^{i\pm1} = \rho_j^i \pm \frac{1}{N}\frac{\partial\rho_j^i}{\partial x} + \frac{1}{2N^2}\frac{\partial^2\rho_j^i}{\partial x^2} \pm \cdots.$$

Without loss of generality, we use ρ_j instead of ρ_j^i as there is no kind of inhomogeneity concerning bulk sites to get

$$\frac{\partial}{\partial t'}\begin{bmatrix}\rho_1\\ \rho_2\\ \rho_3\end{bmatrix} + \frac{\partial}{\partial x}\begin{bmatrix}-\frac{\epsilon}{2}\frac{\partial\rho_1}{\partial x} + \rho_1(1-\rho_1)\\ -\frac{\epsilon}{2}\frac{\partial\rho_2}{\partial x} + \rho_2(1-\rho_2)\\ -\frac{\epsilon}{2}\frac{\partial\rho_3}{\partial x} + \rho_3(1-\rho_3)\end{bmatrix} = S, \tag{6}$$

with

$$S = \begin{bmatrix} \Omega_a(1-\rho_1) - \Omega_d\rho_1 - P + Q \\ \Omega_a(1-\rho_2) - \Omega_d\rho_2 - T + P - Q + R \\ \Omega_a(1-\rho_3) - \Omega_d\rho_3 + T - R \end{bmatrix},$$

$$P = \Omega_1\big(\rho_1^2(1-\rho_2)\big),$$
$$Q = \Omega_2\big(\rho_2^2(1-\rho_1)\big),$$
$$R = \Omega_2\big(\rho_3^2(1-\rho_2)\big),$$
$$T = \Omega_1\big(\rho_2^2(1-\rho_3)\big).$$

Since our main aim is to explore the role of the asymmetric coupling rate, therefore, to simplify the analysis, we restrict our investigation to a specific choice of LK rates. In this study, we focus on the case when $\Omega_a = \Omega_d$, under which the stationary density equations reduce to

$$\frac{\epsilon}{2}\frac{d^2\rho_1}{dx^2} + (2\rho_1 - 1)\left(\frac{d\rho_1}{dx} - \Omega_d\right) - P + Q = 0, \quad (7)$$

$$\frac{\epsilon}{2}\frac{d^2\rho_2}{dx^2} + (2\rho_2 - 1)\left(\frac{d\rho_2}{dx} - \Omega_d\right) + P - T + R - Q = 0, \quad (8)$$

$$\frac{\epsilon}{2}\frac{d^2\rho_3}{dx^2} + (2\rho_3 - 1)\left(\frac{d\rho_3}{dx} - \Omega_d\right) + T - R = 0 \quad (9)$$

with boundary conditions $\rho_1(0) = \rho_2(0) = \rho_3(0) = \alpha$ and $\rho_1(1) = \rho_2(1) = \rho_3(1) = 1 - \beta = \gamma$.

In the past, the singular perturbation technique has successfully explained the rich phase diagrams of coupled TASEP systems with LK; therefore, we exploit the same method to obtain the steady-state solution of the above nonlinear system of equations [24]. One can follow Ref. [30] for a comprehensive description of the approach.

III. RESULTS AND DISCUSSION

To explore the role of lane-changing rates on the steady-state system properties of three-lane TASEP, we define a parameter K, namely, coupling strength [24] (also called the coupling constant [31]), which is the ratio of coupling rates Ω_1 and Ω_2. For simplicity, throughout this paper, we call K the coupling strength. Previous studies have analyzed the impact of K in a two-lane system [31] and reported different values of Ω_1, and Ω_2, with fixed K, leading to different phase diagrams affecting the system dynamics significantly. Apart from that, one study has been conducted on three-lane TASEP without LK with asymmetric coupling conditions [11]. Therefore our aim is not only to understand the influence of K on system dynamics but also to visualize the role of LK in the proposed system. To do this, we calculate the phase diagrams for the same values of K, Ω_1, and Ω_2, which have been used in previous studies so that we can compare the results and can understand the influence of various incorporated processes [11,31] in proposed model dynamics. These observations stimulate the need to explore a few questions as follows: (i) What is the impact of K on phase diagram? (ii) Does the same K with different coupling rates produce the same phase diagram? (iii) How does the LK influence the properties of the phase diagram? and (iv) What are the similarities and differences between the proposed model and corresponding two-lane model? To answer the above questions, we calculate various important characteristics, including phase diagrams, density profiles, and phase transitions for varied important parameters. Refer to Appendix A for the procedure to calculate the phase diagram. Further, $K = 1$ represents a trivial case of symmetric coupling discussed in Appendix B. Similarly, $K = 0$ means a fully asymmetric coupling case which was already discussed in [28]; therefore, we skip this discussion here.

A. Phase diagrams

To begin, we first review the notation of density profiles in each phase diagram in Fig. 2. The density profile takes the form $X_1/X_2/X_3$, with the phases in lane 1, lane 2, and lane 3 denoted by X_1, X_2, and X_3, respectively. X_1, X_2, X_3 can take any one or a combination of basic profiles L (low density with $\rho < 0.5$), H (high density with $\rho > 0.5$), M (maximal current with $\rho = 0.5$), and S (shock phase; sudden change from low density to high density), and D (double shock in a single lane). Note that the phase classification is adopted as the standard definition of low density, high density, and maximal current from past literature [32,33].

As discussed earlier, a past study [24] has proposed understanding the impact of coupling strength (K) on the two-lane TASEP with LK. We calculate the phase diagrams for the same parameters as in [24] to know how system properties alter with the third lane. In Fig. 2(a), the phase diagram with $K = 4$, $\Omega_1 = 0.8$, and $\Omega_2 = 0.2$ is displayed. At this stage, we observe 17 distinct steady-state profiles: $L/L/L$, $L/S/S$, $S/S/S$, $L/L/S$, $L/A/S$, $S/A/S$, $S/LH/S$, $S/S/H$, $L/LML/H$, $L/A/H$, $S/A/H$, $S/LH/H$, $L/HMH/H$, $S/HMH/H$, $L/HL/H$, $S/H/H$, and $H/H/H$. Here LML (density profile, which goes from low density to maximal current and back to low density), HMH(density profile goes from high density to maximal current to high density), LH(density profile with gradual change from low to high density), HL(density profile goes from high-density profile to low-density profile), and A (density profile goes from low density to maximal current to high density) are mixed phases with A as a unique phase which consists of all three basic phases L, M, and H, which is usually rare to find in TASEP-based studies. Further, we notice that phases like $L/L/L$, $S/S/S$, and $H/H/H$ are similar to those observed in the phase diagram for a two-lane system [24], while all remaining phases arise due to dissimilarity between a three- and two-lane system. The third lane produces a complex phase diagram and leads to 17 phases compared to six phases in a two-lane system. Most of the profiles in the second lane are mixed profiles arising due to the impact of the third lane in our system. Since more particles move to the third lane as $\Omega_1 = 0.8$ is higher than $\Omega_2 = 0.2$, the density in the third lane usually remains higher than the other two lanes.

Besides, if we keep $K = 4$ fixed but change $\Omega_1 = 80$, and $\Omega_2 = 20$ as adopted in the two-lane system, we realize that despite fixed K, the phase diagram changes, which was also noticed in [24]. In this case, the phase diagram becomes more

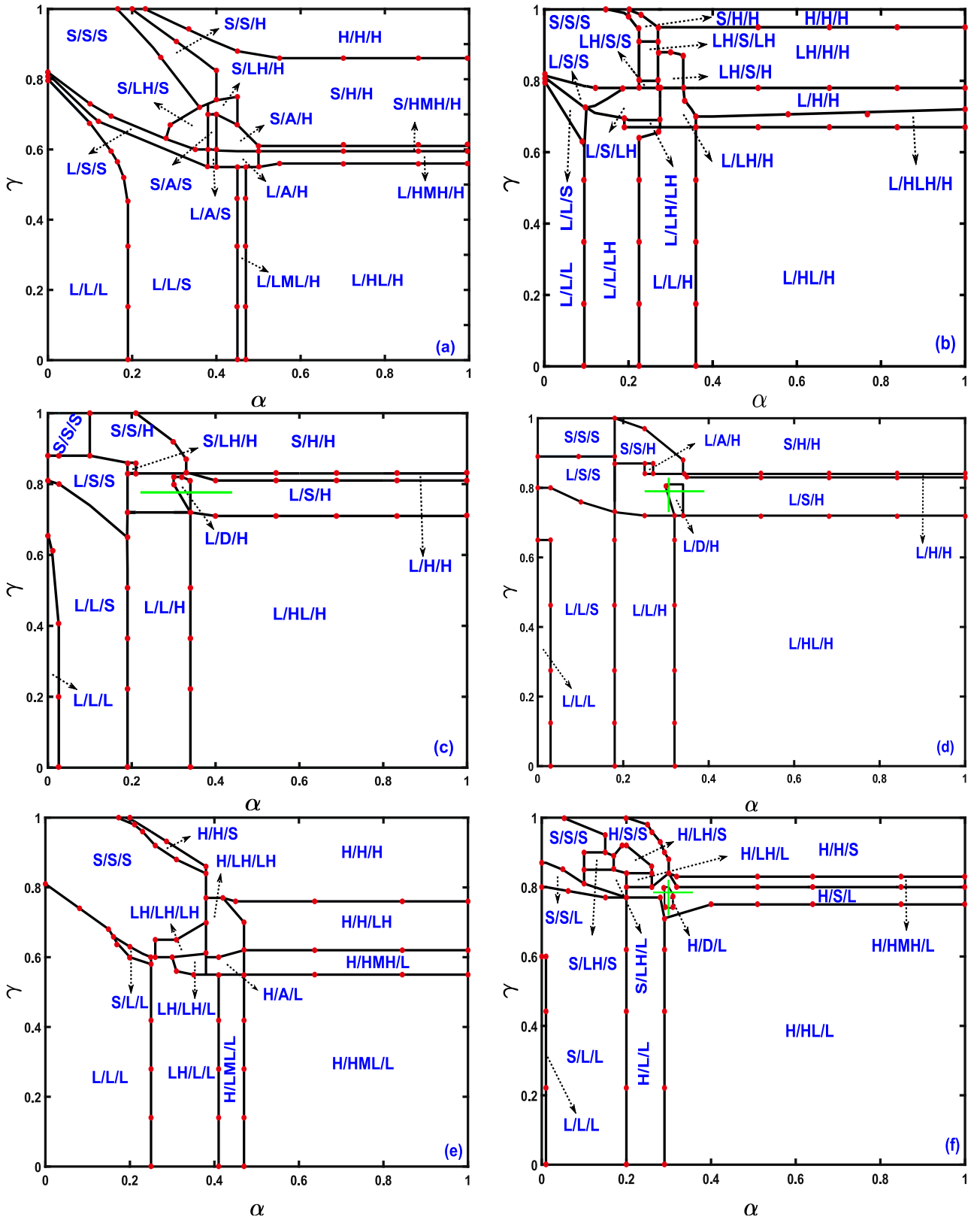

FIG. 2. Phase diagrams for varied coupling strength $K = \frac{\Omega_1}{\Omega_2}$ as (a) $K = 4$, $\Omega_1 = 0.8$, and $\Omega_2 = 0.2$; (b) $K = 4$, $\Omega_1 = 80$, and $\Omega_2 = 20$; (c) $K = 100$, $\Omega_1 = 10$, and $\Omega_2 = 0.1$; (d) $K = 1000$, $\Omega_1 =10$, and $\Omega_2 = 0.01$; (e) $K = 0.7$, $\Omega_1 = 7$, and $\Omega_2 = 10$; and (f) $K = 0.05$, $\Omega_1 = 1$, and $\Omega_2 = 20$. Parameters $\Omega_a = \Omega_d = 0.2$, and $N = 1000$ are the same in (a)–(f). Here Ω_1, Ω_2, Ω_a, Ω_d, α, and $\beta = 1 - \gamma$ are coupling rate (lane 1 to lane 2, lane 2 to lane 3), coupling rate (lane 3 to lane 2, lane 2 to lane 1), attachment rate, detachment rate, entry rate, and exit rate, respectively. Black solid lines are the phase boundaries obtained by mean-field theory (MFT), while red markers correspond to Monte Carlo simulation (MCS) results. The green solid line in (c), (d), and (f) indicates the back-and-forth phase transitions.

complex with 18 phases compared to 17 phases for $\Omega_1 = 0.8$ and $\Omega_2 = 0.2$. In a two-lane system, the number of phases has not changed, contrary to the three-lane case displaying the crucial role of the third lane. Phases like $L/L/L$, $H/H/H$, and $S/S/S$ are similar in this phase diagram and in the phase diagram for the two-lane system, while all remaining phases are not reported in the two-lane system.

In general, the differences between the two-lane model and the proposed model can be explained as follows. In a three-lane system, the middle lane involves a few extra transitions, including particle exchange through lane 1 and lane 3, which make it different from the other two lanes leading to various mixed phases in this lane, as can be seen in Figs. 2(a) and 2(b). Due to the middle lane, a three-lane system produces a very complex phase diagram with many mixed profiles, which are not reported in a two-lane system. Various new phases result in interesting bulk-induced phase transitions, which are discussed in upcoming sections.

Moreover, a past study [11] analyzes a three-lane system in the absence of LK with $\Omega_1 = 10$ and $\Omega_2 = 0.1$. Figure 2(c) shows the phase diagram for the proposed three-lane system with LK and the same coupling rates as in Ref. [11]. It is important to note that LK drastically impacts the topological geometry of the phase diagram leading to the $S/S/S$ phase, which does not exist in the three-lane model without LK. Besides, we notice that one can travel from $L/S/H$ to $L/D/H$ again to $L/S/H$ just by varying $\alpha \in [0.2, 0.4]$ by keeping all parameters fixed with $\gamma = 0.79$. This kind of transition is named a back-and-forth phase transition (also called a reentrance transition), which appears here as a significant impact of LK [34,35]. We discuss it in detail in upcoming sections. The back-and-forth transition is marked using a green line in Fig. 2(c). The reentrance transition that appears in only a small region is a peculiarity of our phase diagram, which can be explained as follows. When the system is in $L/S/H$ and α increases, more particles enter the system, but since $\Omega_1 = 10$ and $\Omega_2 = 0.1$, the flow of particles will be towards lane 3. Since lane 3 is already crowded so it cannot accept more particles, a good number of particles start accumulating in lane 2, leading to another traffic jam near the left boundary resulting in a double shock (D) that transits to high density on further increased in α providing a single shock phase again.

Further, with the different parameter values of $K = 1000$, $\Omega_1 = 10$, and $\Omega_2 = 0.01$ used in Fig. 2(d), we see that there are only 12 distinct density profiles and that the complexity of the profiles is less than in earlier diagrams; however, this phase diagram provides nontrivial features in terms of a double shock (D) in the second lane ($L/D/H$) and a back-and-forth transition as we can start from $L/S/H$ to $L/D/H$ to get $L/S/H$ again just by varying $\alpha \in (0.2, 0.4)$ for fixed $\gamma = 0.76$. Similarly, one can travel from $L/S/H$ to $L/D/H$ again to $L/S/H$ by varying γ from 0.72 to 0.85 with fixed $\alpha = 0.31$. In this way, we observe a two-directional reentrance transition which is not reported in the corresponding two- or three-lane system [11,24,28,31]. The existence of this feature signifies the crucial role of interplay between asymmetric coupling and LK. Note that reentrance transition provides the freedom to control the system dynamics by varying a single parameter. Physically, $L/D/H$ shows two traffic jams in the middle lane, which are undesirable for smooth transportation and can be avoided by varying entry or exit rates due to a reentrance transition. Therefore reentrance transition helps in transiting one phase into other with better control and just by altering a single parameter.

In Fig. 2(e) parameters are $K = 0.7$, $\Omega_1 = 7$, and $\Omega_2 = 10$, and here we have 14 density profiles with the interesting simultaneous double transition from $S/L/L$ changes to $S/S/S$ signifying the transition from L to S in lane 2 and lane 3 together, which was not reported in the corresponding two- and three-lane systems [11,24,28,31]. The double simultaneous phase transition occurs due to the influence of the third lane, LK, and asymmetric coupling and can be explained as follows. When the system is in the $S/L/L$ phase, more particles enter the second and third lanes as the first lane is in the shock phase. On increasing γ, particles tend to stay in that lane for a fixed value of α, which causes the second and third lanes to change to shock simultaneously.

Moreover, for $K = 0.05$, $\Omega_1 = 1$, and $\Omega_2 = 20$, we get 15 density profiles in Fig. 2(f). Here Ω_2 is greater than Ω_1, so the density of particles is high in the first lane. In this phase diagram, we notice the presence of a bidirectional reentrance transition. Fixing α and varying γ, we can see the transition in lane 2 as $H/S/L \to H/D/L \to H/S/L$, and the same transition can be experienced by fixing γ and varying α. This double reentrance transition is indicated by green lines in Fig. 2(f). Another interesting feature of the phase diagram is the existence of phase division as a region of phase $H/D/L$ completely lies inside phase $H/S/L$. It is important to note that to our knowledge, in similar past studies of two- or three-lane systems, no such phase division has been reported showing the critical role of adopted processes in the proposed model.

B. Density profiles and phase transitions

As discussed in previous sections, we obtain phase diagrams and other characteristics utilizing the mean-field approach. To validate these findings, we use Monte Carlo simulations (MCS) which are carried out for $N = 1000$. We perform simulations for 10^{10} times and ignore the first 5% time steps to guarantee the occurrence of a stationary state (Fig. 3). The average density in all three lanes is calculated using time averages over an interval of $10N$. With a margin of error of less than 1%, the phase boundaries are determined.

We have illustrated some of the important stationary density profiles in Fig. 3 obtained using mean-field theory and their validation using Monte Carlo simulations. It is clear from Fig. 3 that there is good agreement between our theoretical outcomes and the simulation results. It is important to note that some of the profiles were not reported in past studies in corresponding two-lane or three-lane systems [11,24,28]. Further, phases like maximal phase M, the mixed profiles LML, HMH, HL, the unique phase A [Fig. 3(a)], and the double shock D [Fig. 3(b)] were not reported in a two-lane system with the same rules [24], which signifies the crucial impact of the third lane on the system dynamics. Similarly, phases like HMH [Fig. 3(c)], LML [Fig. 3(d)], the unique phase A Fig. 3(e)], and LH [Fig. 3(f)] were not reported in a three-lane system without LK [11] indicating the nontrivial impact of LK in our model. Besides, asymmetric coupling present in our model leads to a few new phases, such as

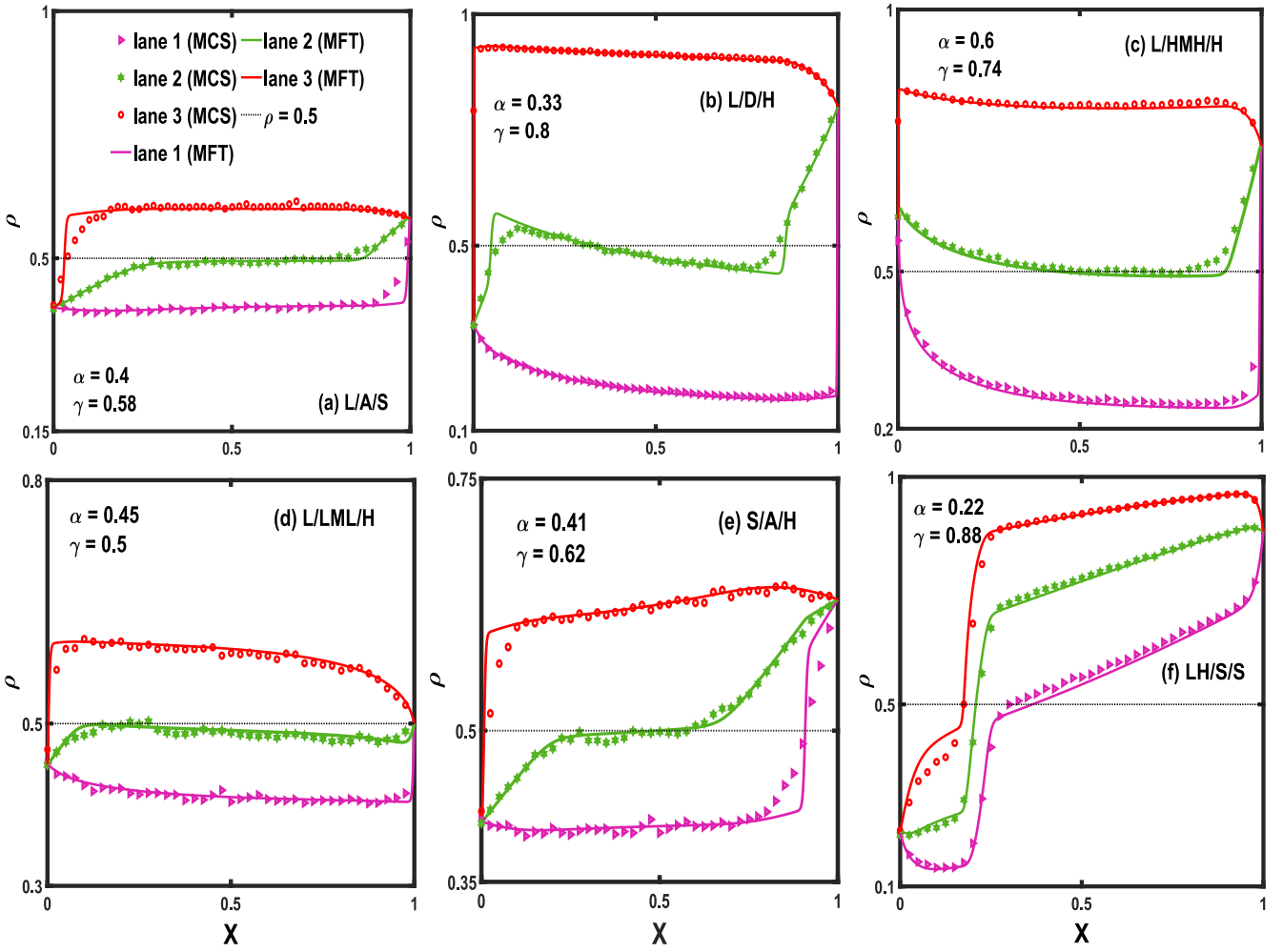

FIG. 3. Density profiles for (a) $K = 1000$, $\Omega_1 = 10$, and $\Omega_2 = 0.1$; (b) $K = 4$, $\Omega_1 = 0.8$, and $\Omega_2 = 0.2$; (c) $K = 4$, $\Omega_1 = 0.8$, and $\Omega_2 = 0.2$; (d) $K = 4$, $\Omega_1 = 0.8$, and $\Omega_2 = 0.2$; (e) $K = 4$, $\Omega_1 = 0.8$, and $\Omega_2 = 0.2$; and (f) $K = 4$, $\Omega_1 = 80$, and $\Omega_2 = 20$. $\Omega_a = \Omega_d = 0.2$, $N = 1000$ are the same in (a)–(f). Here K, Ω_1, Ω_2, Ω_a, Ω_d, α, and $\beta = 1 - \gamma$ are coupling strength, coupling rate (lane 1 to lane 2, lane 2 to lane 3), coupling rate (lane 3 to lane 2, lane 2 to lane 1), attachment rate, detachment rate, entry rate, and exit rate, respectively. The black dotted line represents $\rho = 0.5$.

HMH and LML, which were not reported in the study of three lanes fully asymmetric system with LK. For the sake of completeness and to understand how particles flow along all lanes in steady state, many other density profiles are listed in Appendix C.

Moreover, due to complicated dynamics and a few unique mixed phases, the system experiences various interesting features which can be well explained in terms of phase transitions. In this way, we present various nontrivial transitions between different phases in Fig. 4. Note that in the phase diagram for $K = 1000$ with $\Omega_1 = 10$ and $\Omega_2 = 0.01$, the shape of phase boundaries of a few phases such as $L/A/H$ and $L/D/H$ becomes peculiar leading to a unique kind of phase transition, namely, a back-and-forth phase transition (also called a reentrance transition in the literature) where one can start from phase P_1 to P_2 again to P_1 by just varying a single parameter with all other parameters kept as fixed. In phase diagram Fig. 2(d), we can notice a novel feature called a double back-and-forth transition in lane 2. Here one can travel from $L/S/H$ to $L/A/H$ to $S/S/H$ with varying γ (α) for fixed α (γ). It is important to note that it is rare to witness a double back-and-forth transition (in two directions), as visible here, proving the significance of the proposed model. This transition is shown in Fig. 4(a) and Fig. 4(b). For $\gamma = 0.8$, the middle lane is in the shock phase, which gradually transitions into A at $\gamma = 0.84$ and eventually converts back into the S phase ($S \to A \to S$) at $\gamma = 0.88$ without varying any other parameter leading to the back-and-forth transition in the vertical direction with a fixed value of $\alpha = 0.3$ [Fig. 4(a)]. In the same way, we have shown $S \to A \to S$ by varying $\alpha \in (0.18, 0.3)$, and $\gamma = 0.87$ with the remaining parameters as fixed, showing the same type of transition in the horizontal direction as shown in Fig. 4(b). Moreover, in the phase diagram [Fig. 2(f)] with $K = 0.05$, $\Omega_1 = 1$, and $\Omega_2 = 20$, we obtain the same type of double back-and-forth transition from $H/S/L$ to $H/D/L$ to $H/S/L$ as illustrated in Fig. 4(c) and Fig. 4(d). In Fig. 4(c) the middle lane experiences an S phase at $\gamma = 0.72$ which reaches into the D phase at $\gamma = 0.76$ to finally convert into the shock phase at $\gamma = 0.82$ where the value of $\alpha = 0.32$ is fixed, which shows the transition in the vertical direction.

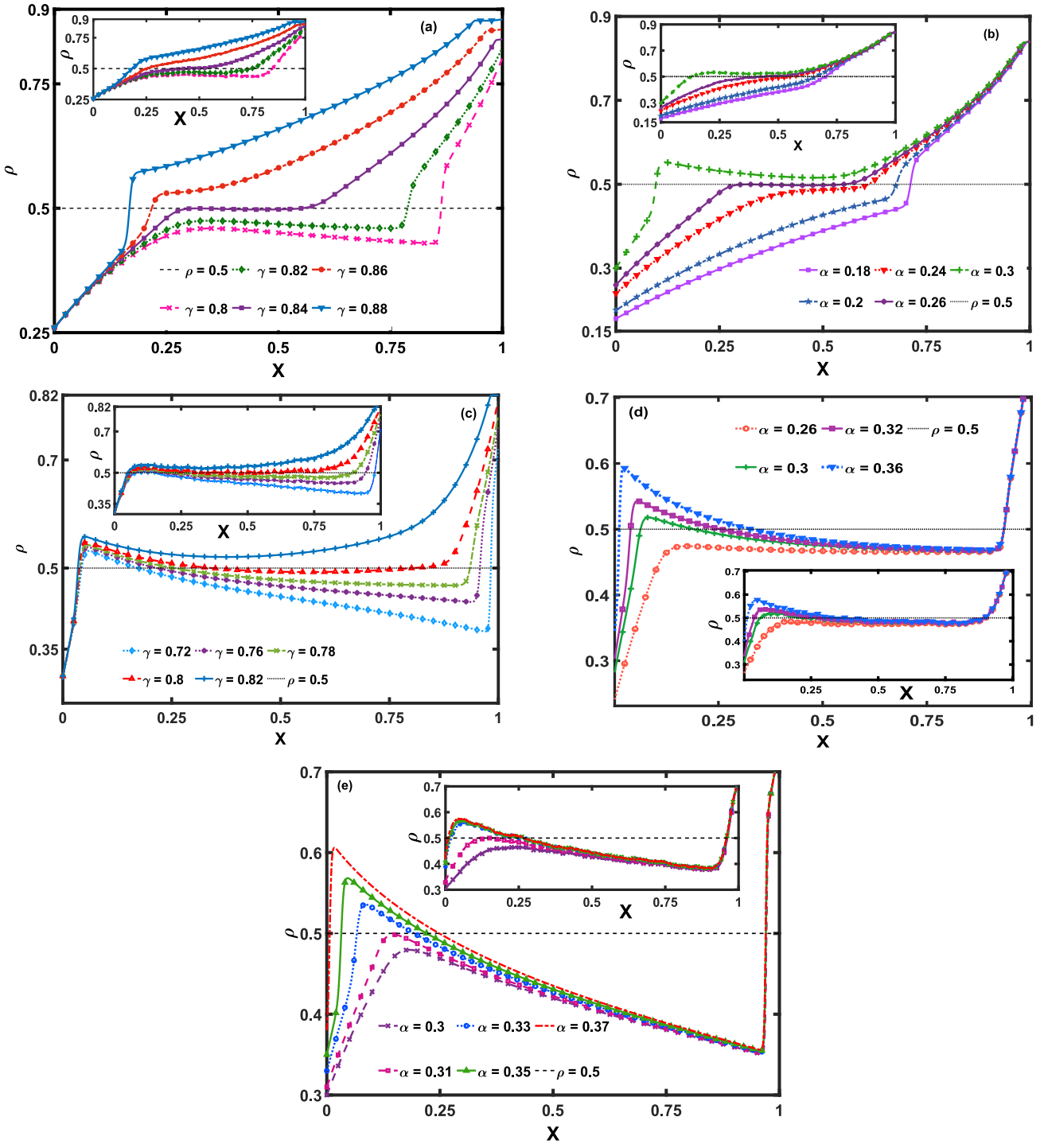

FIG. 4. Phase transitions in lane 2 as (a) $L/S/H \rightarrow L/A/H \rightarrow L/S/H$ for fixed $\alpha = 0.3$, $K = 1000$, $\Omega_1 = 10$, and $\Omega_2 = 0.01$ with varied γ; (b) $L/S/H \rightarrow L/A/H \rightarrow L/S/H$ for fixed $\gamma = 0.87$, $K = 1000$, $\Omega_1 = 10$, and $\Omega_2 = 0.01$ with varied α; (c) $H/S/L \rightarrow H/D/L \rightarrow H/S/L$ for fixed $\alpha = 0.32$, $K = 0.05$, $\Omega_1 = 1$, $\Omega_2 = 20$ for varied γ; (d) $H/S/L \rightarrow H/D/L \rightarrow H/S/L$ for fixed $\gamma = 0.32$, $K = 0.05$, $\Omega_1 = 1$, and $\Omega_2 = 20$ with varied α; and (e) $L/S/H \rightarrow L/D/H \rightarrow L/S/H$ for $\gamma = 0.79$, $K = 1000$, $\Omega_1 = 10$, $\Omega_2 = 0.01$ with varied α. $\Omega_a = \Omega_d = 0.2$ and $N = 1000$ are common in (a)–(e). The respective insets represent Monte Carlo simulation results. Here (a)–(d) and (e) represent the reentrance transition in two directions and one direction, respectively. Here K, Ω_1, Ω_2, Ω_a, Ω_d, α, and $\beta = 1 - \gamma$ are coupling strength, coupling rate (lane 1 to lane 2, lane 2 to lane 3), coupling rate (lane 3 to lane 2, lane 2 to lane 1), attachment rate, detachment rate, entry rate, and exit rate, respectively. The black dotted line represents $\rho = 0.5$.

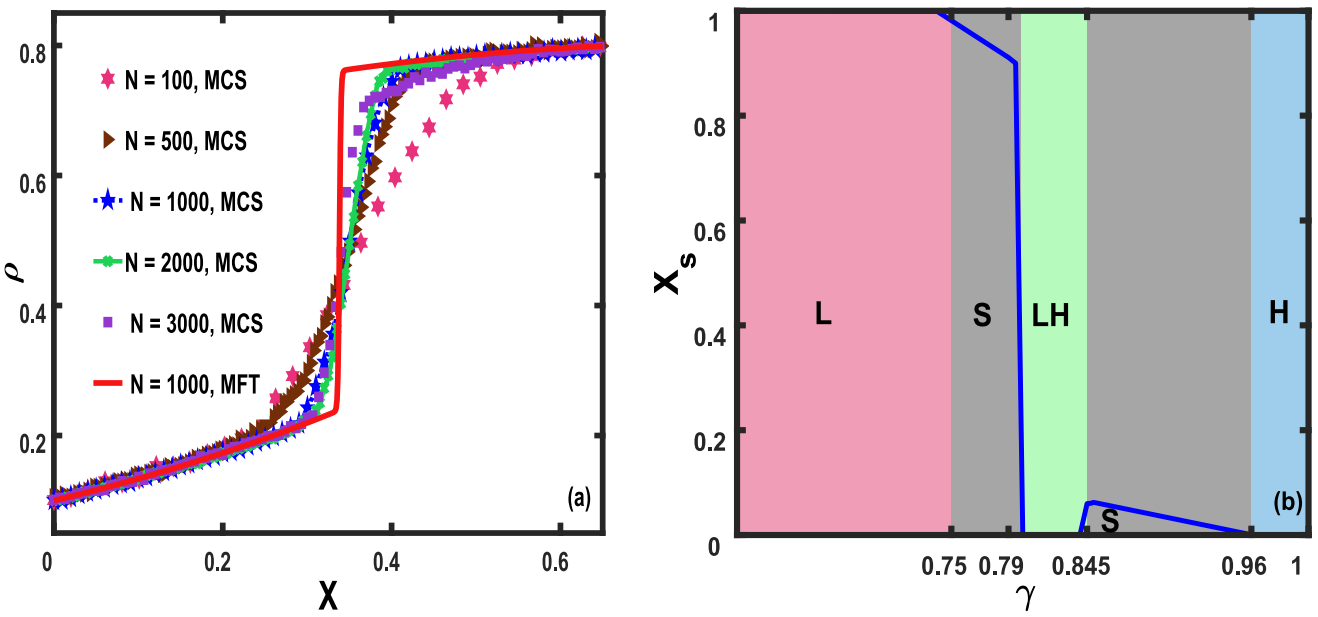

FIG. 5. (a) Finite-size effect on shock profile in lane 3 with $\alpha = 0.1$, $\gamma = 0.75$, $K = 100$, $\Omega_1 = 10$, and $\Omega_2 = 0.1$ for varied N (b) Shock position in lane 2 with $\alpha = 0.26$, $K = 0.05$, $\Omega_1 = 1$, $\Omega_2 = 20$, $\Omega_a = \Omega_d = 0.2$ and $N = 1000$. Panel (b) also signifies the existence of a reentrance transition. Here K, Ω_1, Ω_2, Ω_a, Ω_d, α, and $\beta = 1 - \gamma$ are coupling strength coupling rate (lane 1 to lane 2, lane 2 to lane 3), coupling rate (lane 3 to lane 2, lane 2 to lane 1), attachment rate, detachment rate, entry rate, and exit rate, respectively.

Similarly, the same transition ($H/S/L \to H/D/L \to H/S/L$) is shown in Fig. 4(d) in the horizontal direction by fixing $\gamma = 0.32$ and varying $\alpha \in (0.26, 0.36)$. In the phase diagram [Fig. 2(d)], we observe that one can travel from $L/S/H$ to $L/D/H$ again to $L/S/H$ showing a back-and-forth transition in the middle lane in one direction. Figure 4(e) displays this transition with a fixed value of $\gamma = 0.79$. At $\alpha = 0.3$, the middle lane is in the shock phase, which converts into a double shock at $\alpha = 0.33$ again to achieve the shock phase ($S \to D \to S$) with $\alpha = 0.37$. Since in Fig. 4, transitions take place in the bulk itself, therefore they are called bulk-induced phase transitions.

Moreover, if we compare our model with a two-lane system [24], we can see some of the following similarities. In a two-lane system, only boundary-induced phase transitions are reported, while in the proposed model we have various types of transitions ranging from boundary-induced to bulk-induced to back-and-forth transitions. Two of the common nontrivial transitions between a two-lane system and the proposed model are from $LD \to S$ in the first lane ($\alpha = 0.1$, $\gamma \in [0, 1]$) and $LD \to S \to HD$ [see Fig. 2(a)] in the third lane ($\alpha \in [0, 1]$, $\gamma = 0.1$). The remaining transitions discussed in our model are absent in a two-lane system. Furthermore, all back-and-forth transitions are shown in the middle lane because it differs from the first and third lanes and behaves differently, resulting in various new features, as previously discussed. On the other hand, though a good number of phases are common with three-lane systems without LK, however, due to the involvement of LK, the geometry of the phase diagram changes, which produces a few exciting features and transitions which are not reported in past studies of three lanes. In this direction, the presence of $S/S/S$, transitions involving this phase, bidirectional reentrance transitions, and phase division are a few new features in this model.

1. Finite-size effect and shock dynamics

Here we scrutinize the unique shock features in the proposed three-lane system. The role of the lattice size on the shock profile is also analyzed. From Fig. 5(a) we deduce that the vertical sharpness of the shock profile is enhanced with an increment in lattice size, which proves no finite-size effect is present in the studied system. The absence of a finite-size effect leads to the fact that lattice size does not alter any of the reported features of the system. Since the presence of back-and-forth transitions in the shock phase is one of this study's crucial findings, it is important to investigate the shock dynamics of its position (X_s). In Fig. 5(b), we display the shock position of lane 2 for a fixed value of $\alpha = 0.26$, $\Omega_1 = 1$, and $\Omega_2 = 20$. At $\gamma = 0$, lane 2 is in the L phase with a shock position near one due to a boundary layer at the right end. With an increase in γ, the boundary layer shifts from right to left, producing a shock at $\gamma = 0.741$. Further increasing the value of γ from 0.741, this shock phase transits into a mixed phase LH at $\gamma = 0.799$, which results in a shock position as zero till $\gamma = 0.845$ at which the LH phase converts into a shock phase leading to a nonzero shock position. For $\gamma > 0.845$, the shock phase shifts towards the left, resulting in a high-density phase at $\gamma = 0.96$ with a shock position at 0. Here it is important to note that we observe that one can travel from $S \to LH \to S$ just by varying γ with all other parameters fixed, which proves the existence of back-and-forth phase transitions. Physically, the presence of the back-and-forth transition represents that for a comparatively higher value of γ with fixed entry rate α, lane 2 experiences a traffic jam-like situation which can be avoided just by choosing a suitable value of γ for smooth movement. Mathematically, the both-sided lane switching and LK terms in mean-field equations lead to back-and-forth phase transitions. Therefore, these processes' absence leads to

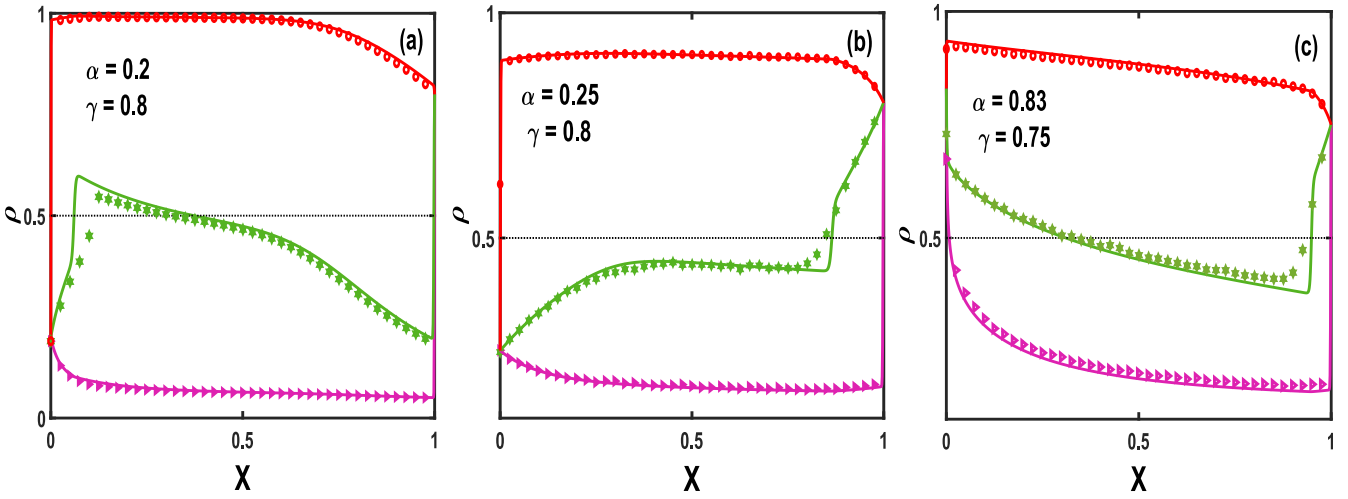

FIG. 6. Three types of shocks profiles. Solid lines indicate mean-field approximation, and markers indicate Monte Carlo simulation outcomes. Here $\Omega_a = \Omega_d = 0.2$, and $N = 1000$. Three profiles indicate $L/S/H$ for (a) $\Omega_1 = 100$, $\Omega_2 = 0.1$; (b) $\Omega_1 = 10$, $\Omega_2 = 0.01$; and (c) $\Omega_1 = 10$, $\Omega_2 = 0.01$. Here K, Ω_1, Ω_2, Ω_a, Ω_d, α, and $\beta = 1 - \gamma$ are coupling strength, coupling rate (lane 1 to lane 2, lane 2 to lane 3), coupling rate (lane 3 to lane 2, lane 2 to lane 1), attachment rate, detachment rate, entry rate, and exit rate, respectively. The black dotted line represents $\rho = 0.5$.

this unique feature's disappearance. Moreover, various kinds of shock phases exist in the present study, as shown in Fig 6. In the first type, there is an abrupt transition from low density to high density and then back to low density [Fig. 6(a)]. The second kind denotes typical shocks [Fig. 6(b)], while in the third type of shock, density changes abruptly from high density to low density before returning to high density [Fig. 6(c)]. Double shock is another attractive shock profile that we discussed previously.

IV. CONCLUSION

In this work, inspired by multilane transport systems, we have studied a three-lane TASEP with LK under the influence of both-sided coupling. Monte Carlo simulations validate the theoretical findings obtained through mean-field analysis. To understand the role of both-sided coupling conditions on system dynamics, various critical stationary characteristics, including phase diagrams, important density profiles, and phase transitions, are calculated utilizing mean-field approximations. The impact of the coupling rates on the phase diagram is also analyzed extensively by defining coupling strength K, which is the ratio of lane-changing rates. The study looks at 51 stationary phases, including 35 mixed phases. Out of these 51 phases, many phases are observed for the first time and were not reported in past studies on two- or three-lane systems. The analysis explains that the both-sided coupling influences the system properties crucially as the same results in various nontrivial and interesting features even for relatively nominal values of coupling strength in the system, which later carries on for its higher value. As we vary the coupling rates, several phases appear and disappear, leading to many nontrivial qualitative and quantitative topological variations in the phase diagram. It is noticed that the comparatively smaller values of coupling strength produce complex phase diagrams with many phases showing that higher sensitivity of the system as even a relatively small variation in the entry or exit rates can change the state of the lattice. Since S and H represent a type of traffic and many phases involve these phases, physically, at this stage, even a minor change in the administrative parameters can enhance or reduce the traffic on the physical or biological paths.

Moreover, the most striking property of the proposed study is the existence of a back-and-forth phase transition in various phase diagrams for $K = 0.05, 100, 1000$. Due to the back-and-forth phase transition, one can travel from $H/S/L$ to $H/D/L$ again to $H/S/L$ just by varying γ in the phase diagram for $K = 0.05$. Surprisingly we also observed that this unique phase transition works in two directions as one can follow $H/S/L$ to $H/D/L$ again to $H/S/L$ by varying α. It is important to note that, to our knowledge, this is the first study on TASEP with back-and-forth transitions in two directions due to the interplay between two-sided coupling and LK in our three-lane system. Similarly, we observe the change from $L/S/H$ to $L/D/H$ again to $L/S/H$ just by varying γ in the phase diagram for $K = 100$ and $K = 1000$. We have also noticed that for $K = 0.05$, phase $H/D/L$ lies entirely inside phase $H/S/L$ leading to a unique phase division. Further, the influence of the system size has been analyzed, and it has been found that lattice size does not affect the reported features of the proposed model.

The proposed model might provide deeper insight into complicated nontrivial dynamics of far-from-equilibrium stochastic transportation systems in the presence of both-sided coupling and Langmuir kinetics and features its crucial impact on system dynamics. In the future, one can generalize this study to incorporate the finite availability of particles, dynamic lattices, bottlenecks, etc.

ACKNOWLEDGEMENT

A.K.V. acknowledges the support from NIT Trichy, India (Grant No. NITT/R&C/SEED GRANT/2021-2022/PROJ.NO.32).

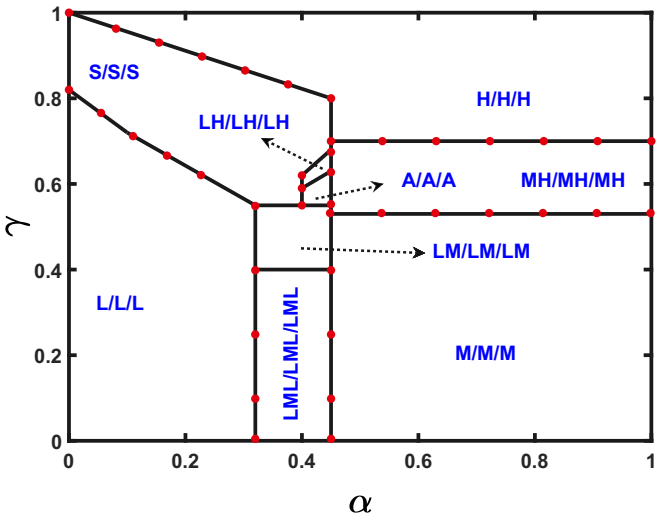

FIG. 7. Phase diagram for symmetric coupling. The black line (red dots) indicated phase boundaries by mean-field theory (Monte Carlo simulations). Here $N = 1000$, $K = 1$, $\Omega_1 = \Omega_2 = 10$, and $\Omega_a = \Omega_d = 0.2$.

APPENDIX A

Here we discuss the procedure to calculate the phase diagrams shown in the main text. The phase diagrams are calculated theoretically using mean-field theory and have been verified through Monte Carlo simulations. One can solve the system of Eqs. (6) to obtain a density profile for a fixed α and γ. By keeping all the parameters fixed, we vary α or γ, and when the phase changes, we notice that α and γ. Similarly, we calculate the density profiles for $\alpha, \gamma \in [0, 1]$ and collect those points at which the phase changes to plot the phase boundaries. In the same way, to plot the phase diagram through simulation (see red dots in each phase diagram), one needs to calculate many density profiles to obtain the (α, γ) at which the phase changes. Further, we can observe that most boundary lines are vertical or horizontal beyond a particular value of α or γ. This is because most phases do not show changes after a particular point by fixing α (or γ) and varying γ (or α).

APPENDIX B

In the main text, we have discussed the system dynamics with asymmetric coupling. For completeness and to compare the outcomes from the main text, here we present the phase diagram with symmetric coupling as displayed in Fig. 7. Due to symmetric coupling, we can see that densities in each lane are the same. We notice nine distinct steady-state profiles: $L/L/L$, $LML/LML/LML$, $M/M/M$, $LM/LM/LM$, $A/A/A$, $LH/LH/LH$, $MH/MH/MH$, $S/S/S$, $H/H/H$ in Fig. 7. Out of the nine, five profiles are mixed, containing maximal current. Compared to phase diagrams shown with asymmetric coupling, we observe that asymmetry enhances the complexity of the phase diagram with more phases leading to various new features absent in the phase diagrams shown in the main text. In general, asymmetric coupling, which is comparatively more realistic to understand transport processes, affects the system dynamics significantly and produces various new phases, reentrance transitions, two parallel transitions, double shock, and phase division, which disappear with symmetric coupling. Moreover, any phase diagram with asymmetric coupling(Fig. 2) provides more than nine phases, as shown in Fig. 7, which signifies that asymmetric coupling affects the system dynamics qualitatively as well as quantitatively. Finally, it is important to note that the phase diagram shown in Fig. 7 remains the same for any value of $\Omega_1 = \Omega_2$.

APPENDIX C

In the main results, we have provided a few main density profiles. For the sake of completeness, we list the remaining density profiles, namely, $L/L/L$, $L/L/S$, $L/S/S$, $S/S/S$, $L/L/H$, $L/H/H$, $S/S/H$, $S/LH/H$, $L/S/H$, $S/H/H$, $H/H/H$, $L/HL/H$, $L/L/LH$, $LH/H/H$, as shown in Fig. 8. Note that all profiles show a good agreement between mean-field analysis and Monte Carlo simulations.

APPENDIX D

In the main results, we have discussed a few phase diagrams with the same coupling strength K but with different values of Ω_1 and Ω_2. It is noticed that the same K produces a different phase diagram. To discuss this, here we present another phase diagram with $K = 4$, $\Omega_1 = 800$, and $\Omega_2 = 200$ in Fig. 9. On comparing this phase diagram with those shown in Figs. 2(a) and 2(b), we notice that the topology of the phase diagram changes again, and the number of phases is reduced due to a higher lane-changing rate. One can derive different phase diagrams with the same K by varying coupling rates. Therefore in the main text, we derived phase diagrams for the same set of parameters adopted in past studies [11,24] so that we can analyze the impact of adopted processes.

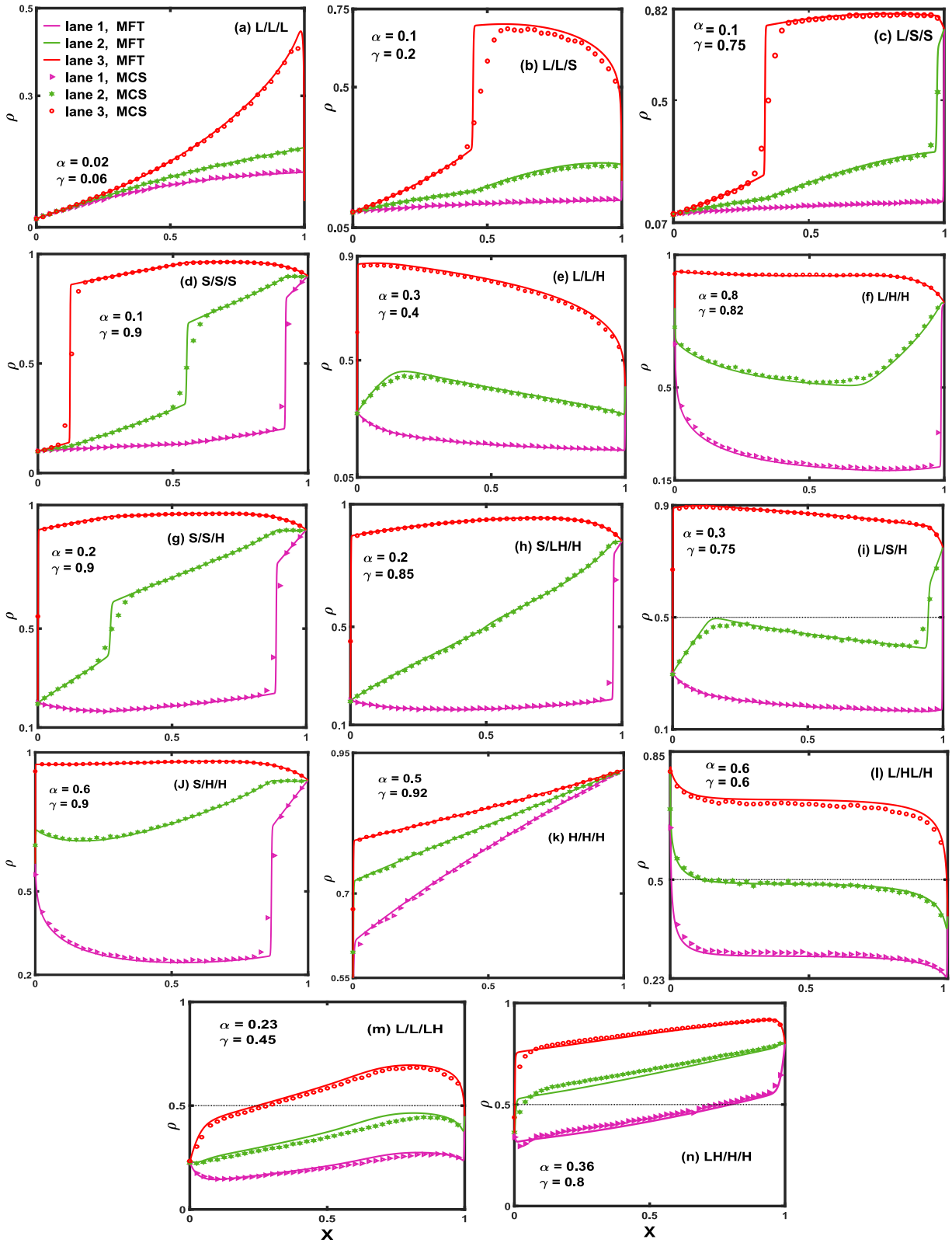

FIG. 8. Density profiles with (a–j) $K = 100$, $\Omega_1 = 10$, $\Omega_2 = 0.1$, (k) $K = 4$, $\Omega_1 = 0.8$, $\Omega_2 = 0.2$, and (l–n) $K = 4$, $\Omega_1 = 80$, $\Omega_2 = 20$. Here $N = 1000$, and $\Omega_a = \Omega_d = 0.2$. The black dotted line is $\rho = 0.5$. Here K, Ω_1, Ω_2, Ω_a, Ω_d, α, and $\beta = 1 - \gamma$ are coupling strength, coupling rate (lane 1 to lane 2, lane 2 to lane 3), coupling rate (lane 3 to lane 2, lane 2 to lane 1), attachment rate, detachment rate, entry rate, and exit rate, respectively.

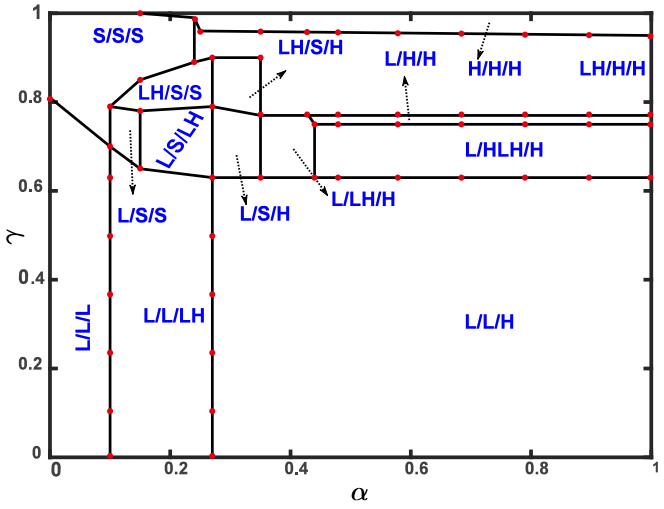

FIG. 9. Phase diagram for $K = 4$. The black line (red dots) indicated phase boundaries by mean-field theory (Monte Carlo simulations). Here $N = 1000$, $\Omega_1 = 800$, $\Omega_2 = 200$, and $\Omega_a = \Omega_d = 0.2$. Here K, Ω_1, Ω_2, Ω_a, Ω_d, α, and $\beta = 1 - \gamma$ are coupling strength, coupling rate (lane 1 to lane 2, lane 2 to lane 3), coupling rate (lane 3 to lane 2, lane 2 to lane 1), attachment rate, detachment rate, entry rate, and exit rate, respectively.

[1] B. Schmittmann and R. K. Zia, Statistical mechanics of driven diffusive systems, Phase Trans. Crit. Phenom. **17**, 3 (1995).

[2] C. T. MacDonald, J. H. Gibbs, and A. C. Pipkin, Kinetics of biopolymerization on nucleic acid templates, Biopolym. Orig. Res. Biomol. **6**, 1 (1968).

[3] D. Chowdhury, L. Santen, and A. Schadschneider, Statistical physics of vehicular traffic and some related systems, Phys. Rep. **329**, 199 (2000).

[4] H. Hilhorst and C. Appert-Rolland, A multi-lane TASEP model for crossing pedestrian traffic flows, J. Stat. Mech.: Theory Exp. (2012) P06009.

[5] T. Karzig and F. von Oppen, Signatures of critical full counting statistics in a quantum-dot chain, Phys. Rev. B **81**, 045317 (2010).

[6] M. Liu, X. Tuo, Z. Li, J. Yang, and Y. Gao, Asymmetric exclusion process for modeling of information flow, Comput. Phys. Commun. **183**, 316 (2012).

[7] S. Klumpp and R. Lipowsky, Traffic of molecular motors through tube-like compartments, J. Stat. Phys. **113**, 233 (2003).

[8] M. Sahoo and S. Klumpp, Asymmetric exclusion process with a dynamic roadblock and open boundaries, J. Phys. A: Math. Theor. **49**, 315001 (2016).

[9] A. F. Yeşil and M. C. Yalabik, Dynamical phase transitions in totally asymmetric simple exclusion processes with two types of particles under periodically driven boundary conditions, Phys. Rev. E **93**, 012123 (2016).

[10] E. Pronina and A. B. Kolomeisky, Spontaneous symmetry breaking in two-channel asymmetric exclusion processes with narrow entrances, J. Phys. A: Math. Theor. **40**, 2275 (2007).

[11] Y.-Q. Wang, R. Jiang, A. B. Kolomeisky, and M.-B. Hu, Bulk induced phase transition in driven diffusive systems, Sci. Rep. **4**, 5459 (2014).

[12] V. Popkov, Boundary driven phase transitions of the first order for systems of conservation laws, J. Stat. Mech.: Theory Exp. (2007) P07003.

[13] M. R. Evans, R. Juhász, and L. Santen, Shock formation in an exclusion process with creation and annihilation, Phys. Rev. E **68**, 026117 (2003).

[14] V. Popkov, A. Rákos, R. D. Willmann, A. B. Kolomeisky, and G. M. Schütz, Localization of shocks in driven diffusive systems without particle number conservation, Phys. Rev. E **67**, 066117 (2003).

[15] J. Krug, Phase separation in disordered exclusion models, Braz. J. Phys. **30**, 97 (2000).

[16] J. Howard and R. L. Clark, Mechanics of motor proteins and the cytoskeleton, Appl. Mech. Rev. **55**, B39 (2002).

[17] A. Parmeggiani, T. Franosch, and E. Frey, Phase Coexistence in Driven One-Dimensional Transport, Phys. Rev. Lett. **90**, 086601 (2003).

[18] A. Parmeggiani, T. Franosch, and E. Frey, Totally asymmetric simple exclusion process with Langmuir kinetics, Phys. Rev. E **70**, 046101 (2004).

[19] A. K. Verma, N. Sharma, and A. K. Gupta, Cooperative motor action to regulate microtubule length dynamics, Phys. Rev. E **99**, 032411 (2019).

[20] E. Pronina and A. B. Kolomeisky, Two-channel totally asymmetric simple exclusion processes, J. Phys. A: Math. Gen. **37**, 9907 (2004).

[21] E. Pronina and A. B. Kolomeisky, Asymmetric coupling in two-channel simple exclusion processes, Physica A **372**, 12 (2006).

[22] A. K. Gupta and I. Dhiman, Coupling of two asymmetric exclusion processes with open boundaries, Physica A **392**, 6314 (2013).

[23] A. K. Gupta and I. Dhiman, Asymmetric coupling in two-lane simple exclusion processes with Langmuir kinetics: Phase diagrams and boundary layers, Phys. Rev. E **89**, 022131 (2014).

[24] I. Dhiman and A. K. Gupta, Effect of coupling strength on a two-lane partially asymmetric coupled totally asymmetric simple exclusion process with Langmuir kinetics, Phys. Rev. E **90**, 012114 (2014).

[25] Z.-P. Cai, Y.-M. Yuan, R. Jiang, M.-B. Hu, Q.-S. Wu, and Y.-H. Wu, Asymmetric coupling in multi-channel simple exclusion processes, J. Stat. Mech.: Theory Exp. (2008) P07016.

[26] Q.-H. Shi, R. Jiang, M.-B. Hu, and Q.-S. Wu, Strong asymmetric coupling of multilane PASEPs, Phys. Lett. A **376**, 2640 (2012).

[27] Y.-Q. Wang, R. Jiang, Q.-S. Wu, and H.-Y. Wu, Phase transitions in three-lane TASEPs with weak coupling, Mod. Phys. Lett. B **28**, 1450123 (2014).

[28] A. K. Verma, A. K. Gupta, and I. Dhiman, Phase diagrams of three-lane asymmetrically coupled exclusion process with Langmuir kinetics, Europhys. Lett. **112**, 30008 (2015).

[29] A. K. Verma and A. K. Gupta, Effect of binding constant on phase diagram for three-lane exclusion process, in *Advanced Computing and Communication Technologies*, Vol. 452 (Springer, Singapore, 2016), pp. 289–296.

[30] S. Mukherji and V. Mishra, Bulk and surface transitions in asymmetric simple exclusion process: Impact on boundary layers, Phys. Rev. E **74**, 011116 (2006).

[31] I. Dhiman and A. K. Gupta, Two-channel totally asymmetric simple exclusion process with Langmuir kinetics: The role of coupling constant, Europhys. Lett. **107**, 20007 (2014).

[32] P. Bonnin, N. Kern, N. T. Young, I. Stansfield, and M. C. Romano, Novel mRNA-specific effects of ribosome drop-off on translation rate and polysome profile, PLoS Comput. Biol. **13**, e1005555 (2017).

[33] A. B. Kolomeisky, G. M. Schütz, E. B. Kolomeisky, and J. P. Straley, Phase diagram of one-dimensional driven lattice gases with open boundaries, J. Phys. A: Math. Gen. **31**, 6911 (1998).

[34] T. Banerjee and A. Basu, Smooth or shock: Universality in closed inhomogeneous driven single file motions, Phys. Rev. Res. **2**, 013025 (2020).

[35] S. Tamizhazhagan, and A. K. Verma, Reentrance transition in two lane bidirectional transport system with bottlenecks, Chaos Solitons Fractals **165**, 112780 (2022).